AMM0023
High Temperature Deformation Behavior of a Newly Developed Mg Alloy Containing Al, Ba and Ca

K.P. Rao[1,*], S.W. Lam[1], N. Hort[2], and H. Dieringa[2]

[1] Department of Mechanical & Biomedical Engineering, City University of Hong Kong, Tat Chee Avenue, Kowloon, Hong Kong
[2] Helmholtz-Zentrum Geesthacht, Institute of Materials Research, Magnesium Innovation Centre, Max-Planck-Straße 1, Geesthacht 21502, Germany
[*] Corresponding Author: mekprao@cityu.edu.hk, +852 3442 8409, +852 3442 0172

Abstract

Newer magnesium alloys that showed promise of high strength and creep resistance are based on Mg-Al-Ba-Ca (ABaX) system. Al, Ba, and Ca are less expensive as alloying elements compared with rare-earth elements and are also flame retarding. ABaX844 is a candidate alloy possessing high creep strength but may pose problems of workability due to heavy alloying. In this study, the deformation characteristics of ABaX844 alloy have been studied using compression tests over a large temperature range of 300 – 500 ^{o}C and strain rate range of 0.0003 – 10 s^{-1} using a 6x6 experimental matrix. The alloy has exhibited two domains for hot working, requiring a minimum temperature of 340 ^{o}C and a strain rate of less than 0.2 s^{-1}. Although the strain rate limit is relatively low compared to many other metallic materials, it is similar to the hot working range of other magnesium alloys that are being used currently. The alloy exhibited extensive dynamic recrystallization resulting in a fine-grained microstructure after hot working in these domains, and the binary and ternary intermetallic phases got well distributed at high temperatures. Also, flow instability manifesting as adiabatic shear band and flow localization occurred at strain rates >0.1 s^{-1}. The mechanical properties of the alloy in the typical service temperature range been evaluated, and it is found that the yield strength and ultimate tensile strength are stable up to 175 ^{o}C.

Keywords: Mg-Al-Ba-Ca alloy; Compressive strength; Flow curves; Hot workability; Microstructure.

1. Introduction

High strength magnesium alloys are normally prepared with alloying additions that include Al, Zn, Sn, Mn and rare-earth elements. However, the high temperature creep strength of such alloys is not satisfactory [1]. Newer alloys that showed promise are based on Mg-Al-Ba-Ca (ABaX) system, where Ba+Ca form thermally stable intermetallic compounds that strengthen the material better than the conventional creep-resistant Mg-Al-RE alloys. Barium in combination with Mg and Al forms a ternary phase $Mg_{21}Al_3Ba_2$ while Ca forms $(Al,Mg)_2Ca$, both occurring independently at grain boundaries in the cast alloys. Quaternary alloys have been developed [2-4] with nominal compositions of Mg-4Al-2Ba-1Ca (ABaX421), Mg-4Al-2Ba-2Ca (ABaX422), and Mg-6Al-3Ba-3Ca (ABaX633) (wt.%). While all these alloys exhibited creep resistance better than AE42, only ABaX633 has shown higher creep resistance than MRI230. The effect of Ba and Ca addition to Mg-Al alloys on strength and elongation showed that the tensile strength increases in the order ABaX211, ABaX422 and ABaX633 [4]. However, they pose the problems of non-uniform precipitate distribution, chemical segregation, micro-porosity and casting defects. Many of these problems can be overcome by thermo-mechanical processing that includes hot working towards obtaining wrought microstructures. The main aim of this research work is to determine the optimal conditions for thermomechanical processing of the newly developed cast ABaX844 alloy to successfully transform it into wrought condition.

2. Preparation and Experimental Procedures

The magnesium alloy Mg-8Al-4Ba-4Ca billet was prepared by conventional casting method using pure elemental metals. The molten alloy was kept at 720 °C under SF6 argon mix cover gas for 10 min before pouring in a preheated permanent steel mold. A cast billet with 100 mm diameter, obtained using the above procedure, was diametrically sliced into disks. Cylindrical specimens of 10 mm diameter and 15 mm of height were machined from the sliced disks of as-cast billet, for compression testing. A hole of 1 mm diameter and 5 mm depth was machined at mid-height to reach the center of the specimen. A thermocouple was inserted in the hole to measure the instantaneous specimen temperature during deformation. The compression testing procedure was described in details earlier [5]. The specimens were subjected to uniaxial compression in the temperature range of 300–500 °C and strain rate range of 0.0003–10 s^{-1}. An exponential decay in the actuator speed of the servo hydraulic machine was applied to achieve constant true strain rates during the compression. Graphite powder mixed with grease was used as the lubricant in all the experiments. The specimens were deformed up to a true strain of about 1 and quenched in water. The deformed specimens were sectioned in the center parallel to the compression axis. The cut surfaces were ground, polished, and etched with dilute nitric acid for obtaining the microstructures. Compression tests were also conducted at a strain rate of 0.001 s^{-1} to obtain the mechanical properties of the alloy in the temperature range 25-250 ^{o}C, in steps of 25 ^{o}C.

3. Results and Discussion

3.1 Initial microstructure

A micrograph of as-cast ABaX844 alloy is shown in Fig. 1. The micro constituents present in this alloy are similar to those analyzed in detail for ABaX alloys [2]. The intermetallic phases consisting of Al, Ba and Ca have been identified to be $Mg_{21}Al_3Ba_2$ and $(Al,Mg)_2Ca$, all of them mainly being present at the grain boundaries in the form of lamelle and block form, respectively. The grain size of the as-cast alloy is in the range of 25-40 µm, and can be considered as fine grained in the case of magnesium alloys.

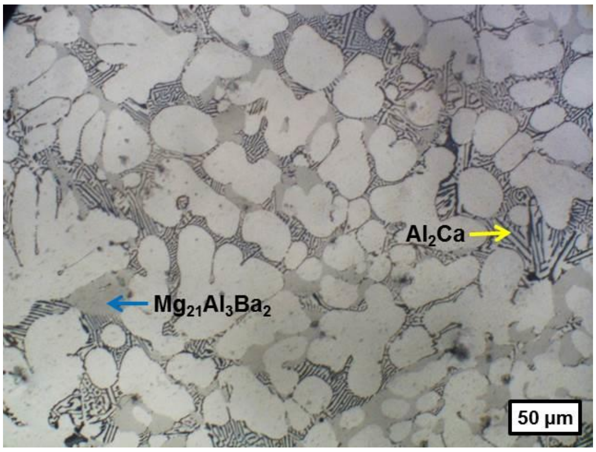

Fig. 1 Microstructure of the as-cast ABaX844 alloy

3.2 Compression behavior and strength

The stress-strain curves obtained from the compression tests of the alloy in the temperature range 25-250 °C are shown in Fig. 2(a). The corresponding values of yield strength (YS) and ultimate compressive strength (UCS) are presented in Fig. 2(b). It can be seen that the alloy is highly brittle up to 75 °C, and has shown a slight increase in plastic deformation up to 200 °C, beyond which it has shown extensive plasticity. The UCS value has gradually decreased from 255 MPa at room temperature to 116 MPa at 250 °C, which are higher than several magnesium alloys. The corresponding YS values are 120 MPa to 75 MPa, with sharper drop beyond 175 °C.

3.3 Deformed specimens and flow curves

The specimens deformed under the several combinations of temperature and strain rates are shown in Fig. 3. It can be seen that a number of specimens have exhibited non-uniform flow or fracture, indicating directly the unsuitability of these conditions for hot working the alloy. All the specimens deformed at the highest strain rate of 10 s^{-1} have shown visible fractures, and those deformed at 300 °C and 340 °C at strain rates of 0.1 s^{-1} and above as well as those deformed at 380 °C has also fractured at 1 s^{-1}. However, the two marked sets of specimens have exhibited very good flow, and will be discussed later along with the microstructural development.

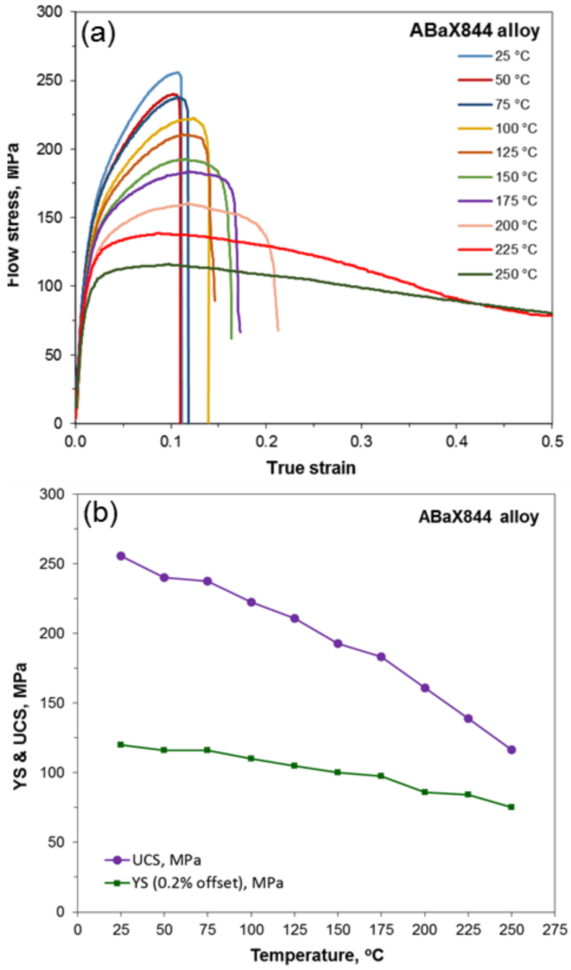

Fig. 2 Flow curves of the ABaX844 alloy at different temperatures and the estimated yield strength and ultimate compressive strength

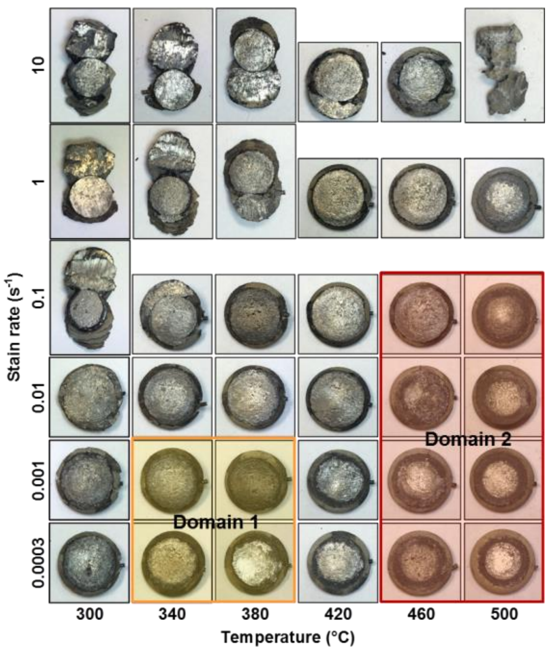

Fig. 3 Shapes of the specimens deformed at different temperatures and strain rates

The load-stroke data were converted into true stress - true strain curves using standard equations. The flow curves corresponding to 340 °C, 420 °C, and 500 °C are shown in Fig. 4 for all the six strain rates. The irregular flow stress variations in Fig. 4(a) reflect the non-uniform flow or fracture of the corresponding specimens shown in Fig. 3. In the case of those deformed at 420 °C and 500 °C, shown in Fig. 4(b) and Fig. 4(c), only those at the highest strain rate of 10 s^{-1} exhibited irregular flow curves. Flow curves at all the other conditions exhibited the characteristics of dynamic recrystallization (DRX), reaching steady-state following a peak in flow stress.

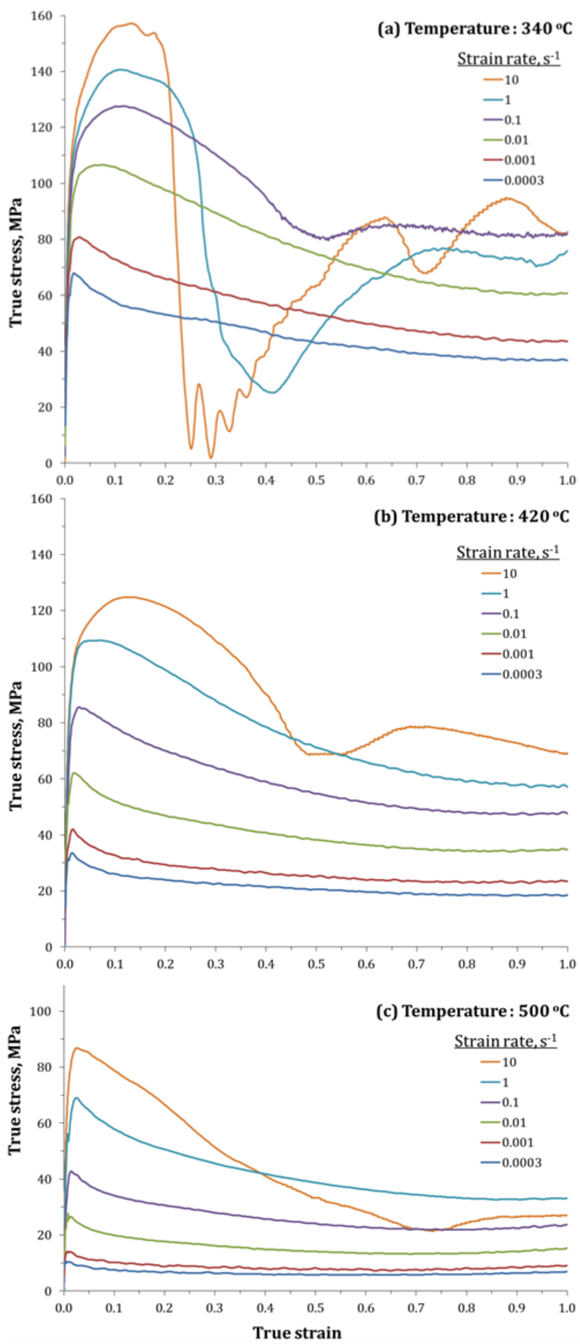

Fig. 4 Flow curves of ABaX844 alloy at (a) 340 °C, (b) 420 °C, and (c) 500 °C for different strain rates

3.4 Processing map

The principles and procedures for the development of processing map are described earlier [5-7]. Briefly, the processing map is a combination of power dissipation map and instability map, which are plotted as variation of power dissipation efficiency (η) and instability parameter (ξ) with temperature and strain rate, respectively. The specimen undergoing deformation is considered to be a non-linear dissipator of power and the strain rate sensitivity (m) of flow stress is the factor that partitions power between deformation heat and microstructural changes. By comparing the power dissipation occurring instantaneously in the specimen with that of an ideal linear dissipator for which the m value is unity, the efficiency of power dissipation during microstructural changes can be calculated using the equation:

$$\eta = 2m/(m+1) \tag{1}$$

The variation of efficiency of power dissipation with temperature and strain rate represents a *power dissipation map*, which is generally viewed as an iso-efficiency contour map. The map exhibits “domains” where the efficiency reaches a peak akin to mountains and separated by valleys representing the change-over from one domain to another. Each of the domains represents a metallurgical mechanism of power dissipation that may be identified on the basis of its characteristics and confirmed by microstructural examination of the deformed specimens.

In view of the irreversibility of large plastic flow, the material undergoes non-uniform deformation under certain conditions of processing and leads to flow instability. The microstructural manifestation of flow instabilities is typically adiabatic shear bands or flow localization. To identify the “regimes” in which the flow becomes unstable or non-uniform, a criterion has been derived by exploring the extremum principles of irreversible thermodynamics as applied to continuum mechanics of large plastic flow [8] and is given by instability parameter $\xi(\dot{\varepsilon})$:

$$\xi(\dot{\varepsilon}) = \frac{\partial \ln[m/(m+1)]}{\partial \ln \dot{\varepsilon}} + m \le 0 \tag{2}$$

The regimes where $\xi(\dot{\varepsilon})$ is negative represent “flow instability” and the variation of the instability parameter (Equation 2) with temperature and strain rate gives a *flow instability map* which may be superimposed on the power dissipation map to give a *processing map*. A processing map thus exhibits domains where the efficiency reaches a peak and regimes of flow instability where the instability parameter is negative. By identifying suitable temperature-strain rate windows for hot working in which microstructurally “safe or good” processes like dynamic recrystallization (DRX) occur and by avoiding flow instability regimes, the workability may be optimized.

The flow stress values were corrected for the adiabatic temperature rise, which was measured during each compression test, to obtain the actual temperature. The corrected flow stress was computed by fitting smooth curves for flow stress data as a function of temperature at all relevant strain rates within the experimental points. The processing map was developed from the variation of corrected flow stress with temperature, strain rate at different strains using the procedure described earlier [5, 6].

The processing maps developed at the strain levels of 0.2 and 0.5, corresponding to the beginning of the deformation and near steady state conditions respectively, are shown in Fig. 5. The numbers associated with the contours represent efficiency of power dissipation in percent.

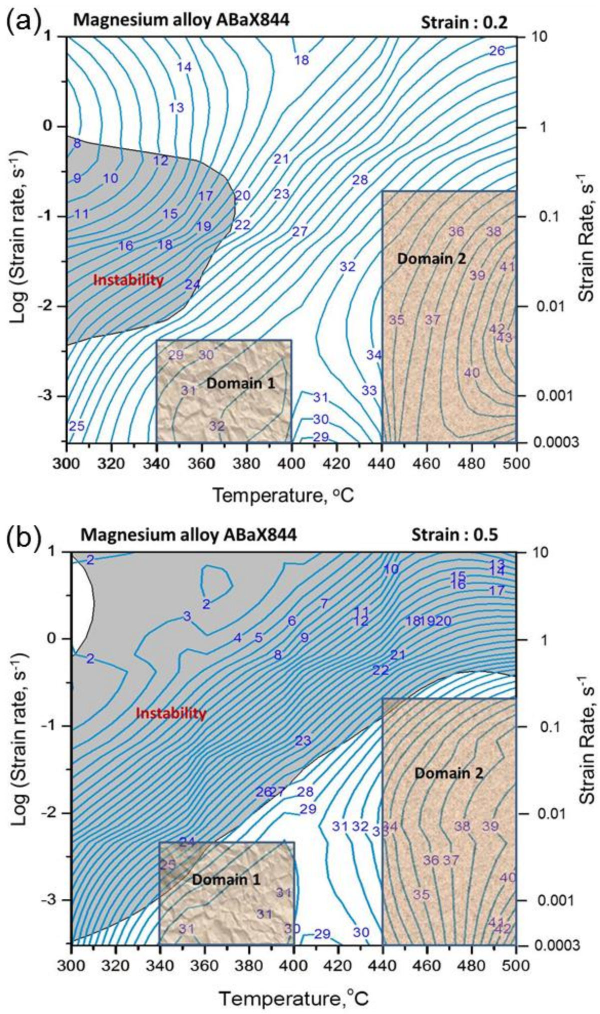

Fig. 5 Processing maps of ABaX844 alloy for two different strain levels

The map in Fig. 5(a) exhibits two domains in the temperature and strain rate ranges: (1) 340 – 400 °C and 0.0003 – 0.005 s^{-1} with a peak efficiency of about 32% occurring in the vicinity of 380 °C, and (2) 440 – 500 °C and 0.0003 – 0.2 s^{-1} with a peak efficiency of about 43% occurring at 500 °C/0.003 s^{-1}. As can be seen from Fig. 5(b), the same two domains continue to exist even at higher deformation level, with a transition from the first domain to the second from 400 °C to 440 °C.

In Domain 1, which is a lower temperature domain, basal slip {0001}<11-20> is highly favored due to its lower CRSS, although prismatic slip {10-10}<11-20> also occurs to a some extent to satisfy the five slip system requirement in polycrystals for continuity of deformation across the grains. As the temperature is increased, the contribution from prismatic slip increases due to lowering of CRSS (critical resolves shear stress) and it dominates deformation in Domain 1. The alloying elements, through solid solution, lower the CRSS for prismatic slip [9, 10], and further promotes its occurrence in Domain 1. The recovery mechanism that operates during deformation by either basal slip or prismatic slip, is the thermal climb process since the mechanical recovery process, cross-slip, is restricted in both cases due to the non-availability of intersecting planes and lower stacking fault energy on the basal planes [11]. However, cross-slip is facilitated in Domain 2 due to higher temperatures, and the activation of a large number of pyramidal slip systems that lead to extensive material flow and dynamic recrystallization. On the basis of instability criterion given by Equation 2, the processing map (Fig. 5) has revealed regimes of flow instability (shaded in gray), and typical ones are marked as “Instability” on the map. It can be noticed that the instability increases as the deformation is continued, as indicated by the larger area of this regime in the map corresponding to the strain of 0.5 as compared to that for the strain of 0.2. The levels of efficiency of dissipation for the respective domains remain nearly the same though the peak for Domain 2 has moved to lower strain rates.

3.5 Validation of processing map

The microstructure obtained on specimen deformed at 380 °C/0.0003 s^{-1} (Domain 1) is shown in Fig. 6. It can be seen that the original cast structure is broken down by the emergence of recrystallized grains.

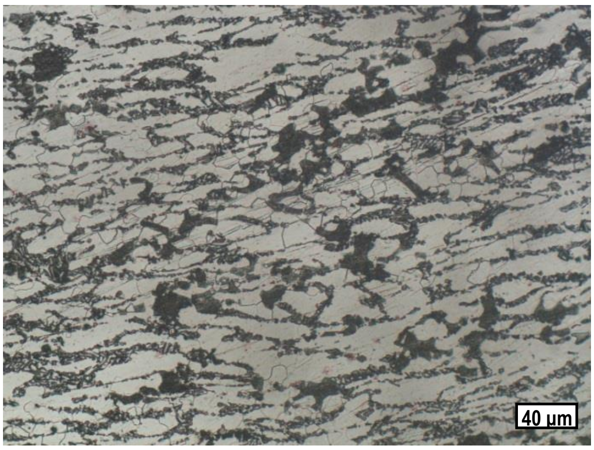

Fig. 6 Microstructure of ABaX844 alloy deformed in Domain 1 of the processing map at 380 °C and strain rate of 0.0003 s^{-1}

ICOME-2016-000326 (this number will be assigned after full manuscript is accepted)

The microstructures obtained on the specimens deformed at 460 °C at the strain rates of 0.01 s^{-1} and 0.0003 s^{-1}, and at 500 °C/0.0003 s^{-1} (all in Domain 2) are shown in Fig. 7. It can be seen that all these conditions facilitated dynamic recrystallization and the breakdown of original network of binary and ternary intermetallic phases. The specimen deformed at the highest temperature 500 °C, shown in Fig. 7(c) shows a fine distribution of the intermetallic phases in the matrix, accomplishing the main objective of hot working so as to obtain uniform properties in the wrought products.

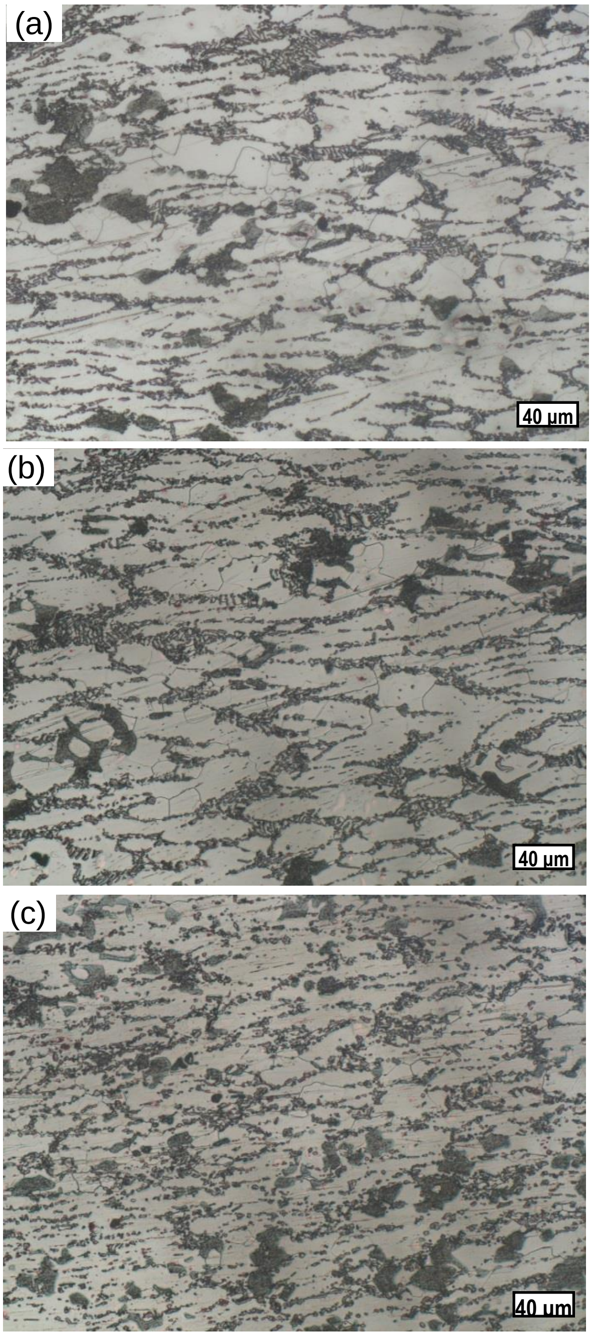

Fig. 7 Microstructure of ABaX844 alloy deformed in Domain 2 of the processing map: (a) 460 °C/0.01 s^{-1} (b) 460 °C/0.0003 s^{-1}, and (c) 500 °C/0.0003 s^{-1}

The microstructure of the specimen deformed in the transition range (420 °C/0.01 s^{-1}) between these domains is shown in Fig. 8. While it also shows the presence of recrystallized grains, the breakdown of intermetallic phases is less extensive, i.e. the microstructure has mixed features of both the domains.

The microstructures of two specimens deformed at instability conditions, as per the processing maps (Fig. 5), are shown in Fig. 9.

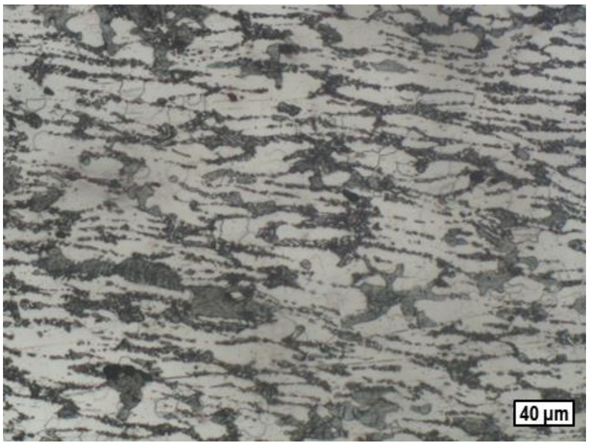

Fig. 8 Microstructure of ABaX844 alloy deformed at 420 °C and strain rate of 0.1 s^{-1}

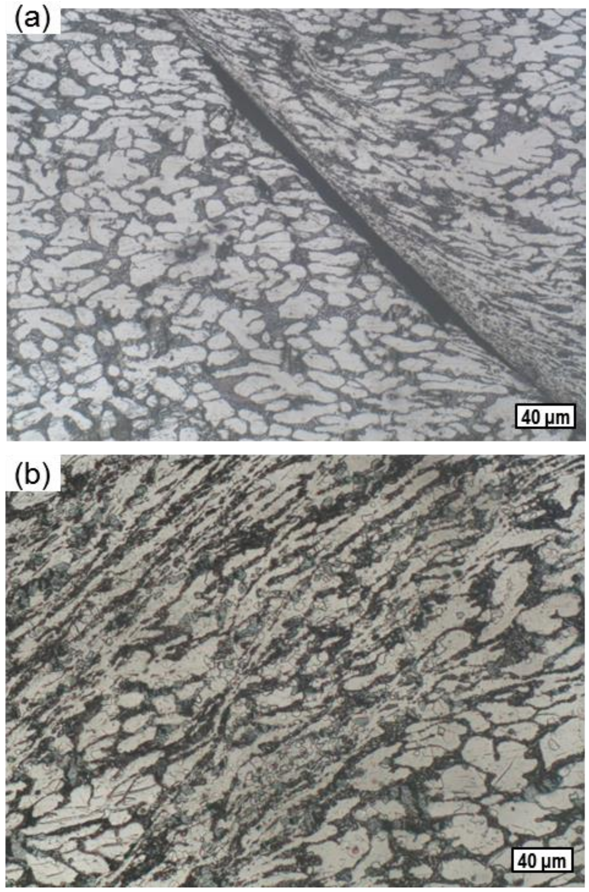

Fig. 9 Microstructure of ABaX844 alloy deformed in the instability regime of the processing map: (a) 300 °C/10 s^{-1} and (b) 300 °C/0.1 s^{-1}

The manifestation of instability in the lower temperature regime is basically localized flow leading to the development of adiabatic shear band in the highest strain rate case, as shown in Fig. 9(a). At lower strain rates in the instability regime, localized flow is prevalent as can be seen in Fig. 9(b). Such flow instability regimes give undesirable microstructures in the hot worked product and therefore have to be avoided in the processing of materials.

4. Conclusions

Mg-8Al-4Ba-4Ca (ABaX844) alloy has been deformed in compression with a view to evaluate its hot working behavior. The following conclusions are drawn from this investigation.

(1) At lower temperatures and higher strain rates, the alloy exhibits flow instability in the form of highly localized material flow, and adiabatic shear bands develop at high strain rates. The flow instability regime also exists at 500 °C at high strain rates.

(2) The processing map developed in the temperature range 300–500 °C and strain rate range 0.0003–1 s^{-1}, exhibited two high efficiency domains in the ranges: (i) 340–400 °C and 0.0003–0.005 s^{-1} and (ii) 460–500 °C and 0.0003–0.2 s^{-1}.

(3) Dynamic recrystallization occurs in both the domains. Basal slip and prismatic slip are dominant flow mechanisms in the first domain, and pyramidal slip is dominant in the second domain. The recovery mechanism leading to dynamic recrystallization is climb of edge dislocations in the first case and cross-slip in the latter at higher temperatures.

(4) In the transition range between the two domains, the microstructure exhibits mixed features.

(5) Although the resultant grain size is slightly larger, the higher temperature domain is preferred in order to achieve high productivity.

(6) The best processing route will be initial large-scale deformation in Domain 2 to convert the alloy into wrought condition and fine distribution of binary and ternary intermetallic phases, followed by secondary or finish forming under the conditions of Domain 1 to obtain fine grain size and high strength.

5. Acknowledgement

The work presented in this paper has been supported by a strategic research grant from City University of Hong Kong (Project Ref. No. 7004454).

6. References

[1] Pekguleryuz, M. and Celikin, M. (2010). Creep resistance in magnesium alloys, *International Materials Reviews*, vol.55, 2010, pp. 197-217.

[2] Dieringa, H., Hort, N. and Kainer, K.U. (2009). Barium as alloying element for a creep resistant magnesium alloy, paper presented in *Magnesium: 8th International Conference on Magnesium Alloys and their Applications,* 2009, Kainer, K.U., Ed., Wiley-VCH Verlag GmbH, Weinheim, pp. 62-67.

[3] Dieringa, H., Huang, Y., Wittke, P., Klein, M., Walther, F., Dikovits, M. and Poletti C. (2013). Compression-creep response of magnesium alloy DieMag422 containing barium compared with the commercial creep-resistant alloys AE42 and MRI230D, *Materials Science and Engineering A*, vol.585, 2013, pp. 430-438.

[4] Dieringa, H., Zander, D. and Gibson, M.A. (2013). Creep behaviour under compressive stresses of calcium and barium containing Mg-Al-based die casting alloys, *Materials Science Forum*, vol.765, 2013, pp. 69-73.

[5] Prasad, Y.V.R.K. and Rao, K.P. (2005). Processing maps and rate controlling mechanisms of hot deformation of electrolytic tough pitch copper in the temperature range 300 – 950 °C, *Materials Science and Engineering A*, vol. 391, 2005, pp. 141-150.

[6] Prasad, Y.V.R.K., Rao, K.P. and Sasidhara, S. (2015). Hot Working Guide: A compendium of processing maps, 2nd edition, ASM, Metals Park.

[7] Prasad, Y.V.R.K. and Seshacharyulu, T. (1998). Modelling of hot deformation for microstructural control, *International Materials Reviews*, vol.43**,** 1998, pp. 243-258.

[8] Ziegler, H. (1965). Paper in *Progress in Solid Mechanics*, Sneddon, I.N. and Hill, R., Eds., vol. 4, John Wiley, New York, pp. 91–193.

[9] Akhtar, A. and Teghtsoonian, E. (1969). Solid solution strengthening of magnesium single crystals - ii the effect of solute on the ease of prismatic slip, *Acta Metallurgica*, vol.17, 1969, pp. 1351-1356.

[10] Blake, A.H. and Caceres, C.H. (2005). Solid Solution effects on the tensile behaviour of concentrated Mg-Zn alloys, paper presented in *Magnesium Technology 2005*, Neelameggham, N.R., Kaplan, H.I. and Powell, B.R., Eds., TMS 2005, Warrendale, pp. 263-267.

[11] Sastry, D.H., Prasad, Y.V.R.K and Vasu, K.I. (1969). On the stacking fault energies of some close-packed hexagonal metals, *Scripta Metallurgica*, vol.3, 1969, pp. 927-930.